Thin Solid Films 518 (2010) 5981–5985

Contents lists available at ScienceDirect

Thin Solid Films

journal homepage: www.elsevier.com/locate/tsf

Interfacial atomic diffusion in AF/Fe/Cu/Fe (AF = $Fe_{50}Mn_{50}$ and $Ir_{50}Mn_{50}$) multilayer systems

V. Kuncser [a,*], W. Keune [b,c], U. von Hörsten [b], G. Schinteie [a], N. Stefan [d], P. Palade [a], G. Filoti [a]

[a] National Institute of Materials Physics, P.O. Box MG 7, 77125, Bucharest-Magurele, Romania
[b] Fakultät für Physik, Universität Duisburg-Essen (Campus Duisburg), D-47048 Duisburg, Germany
[c] Max-Plank-Institut für Mikrostrukturphysik, D-06120 Halle, Germany
[d] National Institute for Lasers, Plasma and Radiation Physics, 07712, Bucharest-Magurele, Romania

ARTICLE INFO

Article history:
Received 1 September 2009
Received in revised form 24 April 2010
Accepted 21 May 2010
Available online 1 June 2010

Keywords:
Interfacial atomic diffusion
Multilayers
Conversion Electron Mössbauer Spectroscopy

ABSTRACT

Spin valve like AF/Fe/Cu/Fe (AF = $Fe_{50}Mn_{50}$ and $Ir_{50}Mn_{50}$) multilayer systems have been prepared by molecular beam epitaxy. Thin tracer layers enriched in the ^{57}Fe isotope were artificially grown at the AF/Fe and Fe/Cu interfaces and the interfacial atomic diffusion was observed via ^{57}Fe conversion electron Mössbauer spectroscopy. The results show that the atomic interdiffusion at all involved interfaces is lower in the IrMn based structures as compared to the FeMn based ones.

1. Introduction

Magnetic recording has sharply progressed over the last five decades. The amount of information per unit area has increased by more than seven orders of magnitude, e.g., from 2 kbits/in^2 in 1956 to more than 100 Gbits/in^2 in the present disks [1]. This impressive achievement was connected with an important progress in decreasing the bits (seen as small magnetized regions) as well as in decreasing the size of the writing/reading elements [2]. Today's magneto-resistive elements are based on Giant Magneto-Resistance (GMR) or Tunneling Magneto-Resistance effects [3,4]. The main component of such an element is the spin-valve structure. Among the presently used structures, the most convenient one consists of a stack of ferromagnetic (F), antiferromagnetic (AF) and non-magnetic (NM) metallic thin films [5]. The simplest stack of a GMR based element (which is in fact also its active part) is of type AF/F/NM/F, generally with NM = Cu. The electron transport through the Cu conductive thin layer is controlled via the relative orientation of the spins (or magnetizations) in the adjacent F layers. The switching from the parallel to the antiparallel magnetic configuration of the two F layers is realized via the application of a small magnetic field (e.g., generated by the magnetic bits). The magnetic behavior of the F layer coupled to the AF layer is influenced by the exchange bias effect [6] which is related to the unidirectional anisotropy induced, under certain conditions, at the AF/F interface. Macroscopically, the effect may manifest itself by a negative or positive shift of the hysteresis loop of the coupled F layer as well as by an increased coercivity (the latter being connected with a uniaxial anisotropy). The shift of the loop from zero field is called exchange bias field, H_E. Therefore, the complex loop of the above mentioned spin-valve structure can be decomposed into the shifted hysteresis loop of the coupled F layer and the loop of the free F layer which is centered at zero field. During the magnetization reversal process, the spin orientation in the two F layers can be similar or opposite, depending on the value of the applied field with respect to H_E. The exchange bias field, as one of the crucial parameters of a spin-valve structure, may be roughly expressed via the relationship: $H_E = \sigma / M_r t$ where σ is the interfacial exchange energy, M_r the remanent magnetization of the pinned F layer and t its thickness [1]. Evidently, both the interfacial exchange energy and the remnant magnetization depend on many other variables such as the type of the F and AF films, their crystalline structure and phase composition, the quality of the AF/F interface, etc. [7–10]. In addition, also the electron transport through the conductive layer can be drastically influenced by the F/Cu interface on the both sides of the Cu layer. Hence, the quality of all interfaces of the multilayer structure becomes of main importance in regard to different aspects of its GMR behaviour. Convenient AF pinning layers in giant magneto-resistive elements consist in either equatomic Fe–Mn alloys with fcc structure or in Mn rich Ir–Mn alloys with similar structure, but with a relatively improved corrosion resistance and lower critical thickness. The present paper deals with a study of the interfacial atomic diffusion mechanisms in stacks of type AF/Fe/Cu/Fe, by ^{57}Fe conversion electrons

* Corresponding author. Tel.: +40 21 369 01 85; fax: +40 21 369 01 77.
E-mail address: kuncser@infim.ro (V. Kuncser).

0040-6090/$ – see front matter © 2010 Elsevier B.V. All rights reserved.
doi:10.1016/j.tsf.2010.05.100

Mössbauer spectroscopy (CEMS). Tracer layers of ^{57}Fe were inserted on the ferromagnetic side at either the interface with the AF layer or with the Cu conductive layer. Equiatomic compositions of types $Fe_{50}Mn_{50}$ and $Ir_{50}Mn_{50}$ were considered for the AF films in order to have a unitary picture with respect to interfacial diffusion phenomena at the AF/Fe interface. Spin configurations and interfacial diffusion mechanisms in exchange bias and spin-valve structures with Ir–Mn antiferromagnetic pinning layers were reported also in [11]. Those systems were prepared by rf. sputtering, resulting in more defected Fe layers as compared to the structures presented in the following. The overall Fe layer was enriched in ^{57}Fe and not only an interfacial tracer layer, since the aim of that earlier study was to observe the phase composition of the Fe layers interfaced (down-top; top-down) to Cu or Ir–Mn layers with high Ir content.

2. Experimental details

The layered structures were grown on commercial Si substrates by molecular beam epitaxy (MBE). The substrates were rinsed in acetone and subsequently in ethanol, just before loading into the vacuum chamber, where they were cleaned by sputtering with low energy argon ions (ion energy, current density and argon pressure of 500 eV, 1 μA/cm^2 and 5.5×10^{-5} mbar, respectively). A Cu buffer layer (15 nm thick) was initially grown at 100 °C and then the AF thin films (15 nm thick) were deposited by co-evaporation from two sources at a pressure of 8×10^{-10} mbar during deposition (base pressure of 3×10^{-10} mbar). Subsequently, Fe/Cu/Fe layers were grown with deposition rates ranging from 0.2 to 0.5 nm/min, depending on the type of film. With exception of the Ir metal, which was evaporated via an electron gun, all the other components were evaporated from Knudsen cells. The evaporation rates were monitored with a calibrated quartz-crystal microbalance; in the case of the AF films they correspond to the equiatomic composition of Fe–Mn or Ir–Mn. Tracer layers of ^{57}Fe were deposited at different interfaces of the structures, and finally the thin-film stacks were protected by 5 nm thick Cu cap layers. Six different systems were prepared in this way, with the following geometrical structure (see also Fig. 1 with AF = FeMn and IrMn, respectively):

Sample FeMn_02 : Si/Cu(15nm)/$Fe_{50}Mn_{50}$(15nm)/^{nat}Fe(3.5nm) /^{57}Fe(1.5nm)/Cu(5nm)/^{nat}Fe(5nm)/Cu(5nm)

Sample FeMn_03 : Si/Cu(15nm)/$Fe_{50}Mn_{50}$(15nm)/^{57}Fe(1.5nm) /^{nat}Fe(3.5nm)/Cu(5nm)/^{nat}Fe(5nm)/Cu(5nm)

Sample FeMn_04 : Si/Cu(15nm)/$Fe_{50}Mn_{50}$(15nm)/^{nat}Fe(5nm)/Cu(5nm) /^{57}Fe(2nm)/^{nat}Fe(3nm)/Cu(5nm)

Sample IrMn_02 : Si/Cu(15nm)/$Ir_{50}Mn_{50}$(15nm)/^{nat}Fe(3.5nm) /^{57}Fe(1.5nm)/Cu(5nm)/^{nat}Fe(5nm)/Cu(5nm)

Sample IrMn_03 : Si/Cu(15nm)/$Ir_{50}Mn_{50}$(15nm)/^{57}Fe(1.5nm) /^{nat}Fe(3.5nm)/Cu(5nm)/^{nat}Fe(5nm)/Cu(5nm)

Sample IrMn_04 : Si/Cu(15nm)/$Ir_{50}Mn_{50}$(15nm)/^{nat}Fe(5nm)/Cu(5nm) /^{57}Fe(2nm)/^{nat}Fe(3nm)/Cu(5nm).

In the above notation, ^{nat}Fe labels a metallic layer grown from natural Fe (mainly ^{56}Fe and only ~2% natural abundance of ^{57}Fe), whereas ^{57}Fe labels a metallic layer grown from Fe enriched to 95% in the ^{57}Fe isotope. It is worth mentioning that the crystalline structure and electronic properties of the ^{57}Fe layer are identical to those of the ^{nat}Fe layer (body centred cubic, bcc), the only difference consisting in those of the enhanced sensitivity of the tracer layer with respect to ^{57}Fe Mössbauer spectroscopy. The density of the Mössbauer events (number of events per volume unit) is proportional to the density of ^{57}Fe nuclei, and hence, it has to be almost 47 times higher in a ^{57}Fe enriched layer with a similar thickness as a natural Fe layer. From the magnetic point of view, one can consider that samples FeMn_02, FeMn_03 and FeMn_04 are all identical, reproducing a spin-valve structure of type AF(15 nm)/F(5 nm)/Cu(5 nm)/F(5 nm). The difference consists only in the position and thickness of the ^{57}Fe tracer layer which is placed at various interfaces, i.e., just below the Cu layer (sample FeMn_02), just above the Cu layer (sample FeMn_04) or just above the AF layer (sample FeMn_03). The second set of three samples is similar to the set of samples just described, the only difference being the use of IrMn instead of FeMn for the AF layer. It is worth mentioning that none of the typical procedures for inducing exchange bias field were applied (biasing magnetic field during the growing process or a subsequent field cooling procedure from above the Néel temperature of the AF film), since the main interest was concentrated on the interfacial atomic diffusion process.

The phase composition and local magnetic interactions within the F layer as well as the atomic interdiffusion processes at the different interfaces were investigated by ^{57}Fe CEMS. The CEMS measurements were performed at room temperature (RT) with a constant acceleration spectrometer and a gas-flow proportional counter with a He–CH_4 mixture. A ^{57}Co-source in a Rh-matrix was used. All spectra were recorded in perpendicular back-scattering geometry, i.e. the incident γ-ray direction was perpendicular to the multilayer plane. The CEMS spectra were fitted using the "NORMOS" package developed by Brand [12]. All isomer shifts (δ) are given relative to bulk α-Fe at room temperature. X ray diffraction studies (Cu-K_α radiation) and Atomic Force Microscopy were performed for a preliminary structural and morphological characterization of the systems.

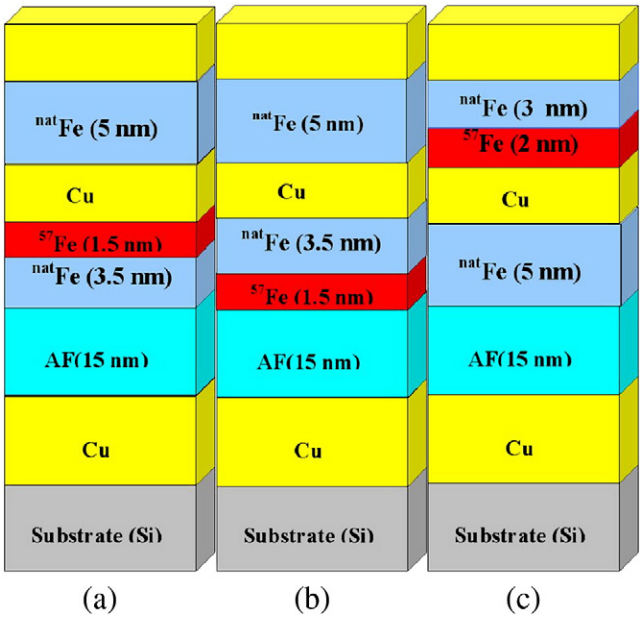

Fig. 1. The geometrical structure of the analyzed systems. From the left side to the right side are shown stacks with the general label AF_02 (a), AF_03 (b) and AF_04 (c). AF can be either $Fe_{50}Mn_{50}$ or $Ir_{50}Mn_{50}$. ^{57}Fe tracer layers were artificially grown at the AF/Fe interface (stack AF_03) or at the Fe/Cu interface (stacks AF_02 and AF_04).

3. Results and discussions

The Cu buffer layer has promoted a face centred cubic (fcc) structure for both $Fe_{50}Mn_{50}$ and $Ir_{50}Mn_{50}$ films, as proven by preliminary X ray diffraction measurements using Cu-K_α radiation. Only the diffraction lines from Cu (111) and Fe–Mn (111) at around 43.4 deg (or,

alternatively, Ir–Mn (111) at around 41.4 deg) were observed over the angular interval from 20 to 65 deg, standing for a certain crystallographic texture of the AF phases. Atomic Force Microscopy images evidenced surface morphological entities with an average size of the order of 100 nm and average surface roughness of the order of a few nm for both systems. Therefore, the two-dimensional character of the multilayer structure is assumed to be preserved and the magnetic and electron transport properties of the geometrically identical systems have to depend only on the antiferromagnetic characteristics of the pinning layer and the microscopic quality of the involved interfaces.

The ^{57}Fe Mössbauer spectra obtained at RT on FeMn and IrMn spin-valve structures with ^{57}Fe tracer layers placed at different interfaces are shown in Figs. 2 and 3, respectively. The best fitting was achieved by using three Mössbauer components with Lorentzian line shape: (i) a most intense sharp outer sextet, (ii) a less intense inner sextet and (iii) a relatively broad central paramagnetic singlet, which might be responsible also for broad doublets of weak quadrupole splitting. The linewidths of the outer sextet range between 0.32 and 0.35 mm/s, and of the inner sextet between 0.65 and 0.75 mm/s for all samples. In comparison, the linewidth of the central singlet ranges between 0.85 and 0.95 mm/s, for all samples. The two sextets show negligible quadrupole shifts whereas the isomer shifts relative to α-Fe at RT are close to zero, for all structures. The isomer shift of the singlets is about −0.1 mm/s for FeMn based structures and about +0.15 mm/s for IrMn based ones. At a first view this difference of isomer shifts between the two sets of samples seems to be unexpected, especially in case of samples of type (a) and (c) (see Fig. 1), but in fact it suggests a different Fe aggregation process at the interface, as it will be proven later.

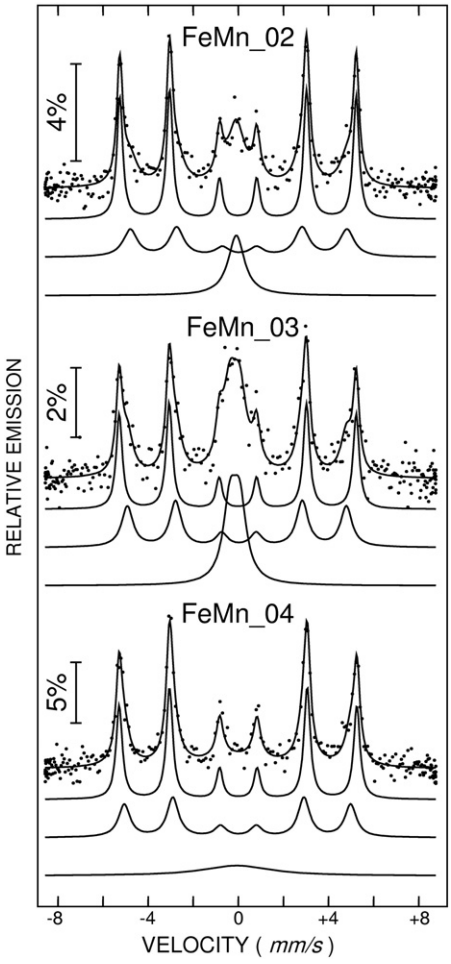

Fig. 2. Mössbauer spectra of spin-valve structures with FeMn antiferromagnetic layers and with different locations of ^{57}Fe tracer layers, measured at room temperature.

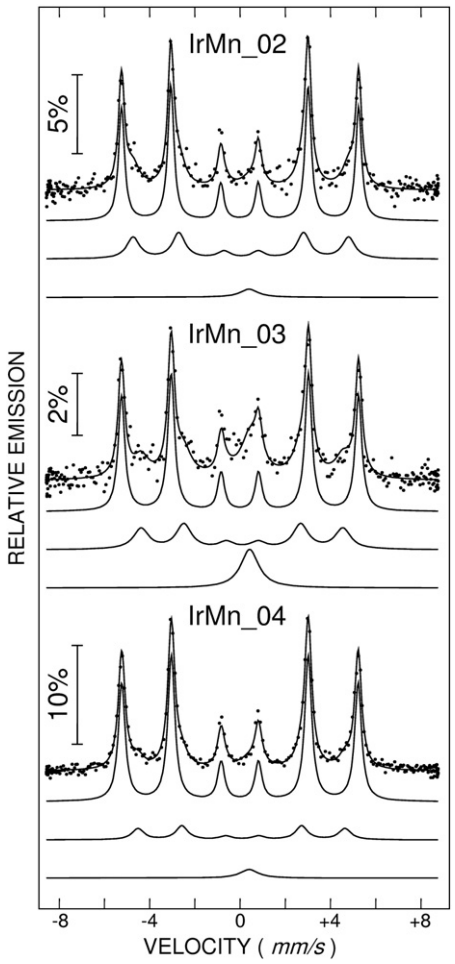

Fig. 3. Mössbauer spectra of spin-valve structures with IrMn antiferromagnetic layers and with different locations of ^{57}Fe tracer layers, measured at room temperature.

The magnetic hyperfine field of the outer sextet is 32.5(2) T whereas that of the inner sextet is about 30.0(5) T in all cases. All these Mössbauer results suggest the conclusion that the outer sextet is due to the next Fe layer away from the interface and will be considered in the following as belonging to a bulk-like Fe layer which is not influenced by interfacial atomic diffusion. The inner sextet, with relatively larger linewidth and lower hyperfine field is due to a defective bcc Fe phase in the direct neighbourhood of the AF/Fe, Fe/Cu or Cu/Fe interfaces and will be considered as sensing the interfacial atomic interdiffusion. This means that the lower magnetic hyperfine field of the inner sextet is due to the presence of Cu (or alternatively Mn) atoms in the bcc structure of the interfacial α-Fe layer. Based on data of Sumiyama et al. [13], a decrease of the magnetic hyperfine field by about 1 T per Cu nearest-neighbour atom, in the Fe rich part (bcc structure) of the Fe–Cu alloy can be considered. Therefore, the values of the hyperfine field in the direct neighbourhood of the Fe/Cu interface (Fe side) are consistent with the presence of two or three Cu atoms in the bcc cell of Fe for both FeMn and IrMn based stacks. Finally, the central component in the IrMn based systems is assigned only to ^{57}Fe nuclei which diffuse from the Fe layer inside either the Cu or the IrMn layer, whereas in the FeMn structures, the central component is attributed to ^{57}Fe nuclei diffusing from the Fe layer inside either the Cu or FeMn layers and, moreover, to the ^{57}Fe nuclei belonging to the AF layer itself (the magnetic hyperfine field of Fe in the FeMn equiatomic composition is so small at room temperature that a magnetically split component cannot be resolved).

The interfacial atomic interdiffusion can be studied in the considered systems via a careful analysis of the CEMS data belonging to the inner

sextet and the central pattern component. The degree of diffusion into or from the ^{57}Fe tracer layer at the interface might be estimated from the relative spectral area of these components in the Mössbauer spectra. The relative spectral area is proportional to the total number of ^{57}Fe nuclei belonging to each phase (a quite similar Debye–Waller factor can be assumed for the involved phases). Because the crystalline structure is different in the Fe layer and in the adjacent neighbouring (Cu, FeMn or IrMn) layers, one has to uniquely interpret the diffusion in terms of equivalent thickness of bcc Fe. For example, in sample IrMn_4, the total number of Fe atoms which penetrate into the fcc Cu conductive layer, is expressed as the number of Fe atoms which belong to a pure layer of bcc Fe of effective thickness t^d_{eff} (effective thickness of diffusing Fe atoms). Similarly, the total number of Fe atoms in the bcc Fe layer, which sense the influence of the Cu atoms, is expressed as the number of Fe atoms which belong to a pure layer of bcc Fe of effective thickness t^p_{eff} (effective thickness of perturbed Fe atoms). The above defined effective thicknesses, related to the atomic interdiffusion processes at the interface, will be estimated in the following by starting from the relative area of the Mössbauer spectral components. At this point it is worth mentioning that the Fe tracer layer at the interface is 95% enriched in the ^{57}Fe isotope and most of the Mössbauer signal originates from this layer (about 82–92% of the total spectral area, depending on the sample). The outer sextet, assigned mainly to that part of the tracer layer which is not influenced by the interfacial diffusion, is the most intense spectral component. Therefore, it is expected that the different effective thicknesses regarding the diffusion process are much lower than the thickness of the tracer layer (t_t). That is, the diffusion process involves almost completely Fe atoms with ^{57}Fe nuclei. Hence, all the above considerations will refer to the effective thickness of bcc Fe layers enriched in ^{57}Fe. Because a part of the Mössbauer signal comes also from layers containing natural Fe (2% ^{57}Fe natural abundance), their spectral contributions will be expressed by equivalent thicknesses of enriched ^{57}Fe layer. The following distinct cases have to be taken into account: (i) samples of type FeIr_02 and FeIr_03 with 1.5 nm ^{57}Fe tracer layer and 8.5 nm natural Fe in both the top and bottom F layers (ii) FeIr_4 with 2 nm ^{57}Fe tracer layer and 8 nm natural Fe, (iii) FeMn_02 and FeMn_03 with 1.5 nm ^{57}Fe tracer layer, 8.5 nm natural Fe and 15 nm FeMn layer and (iv) FeMn_04 with 2 nm ^{57}Fe tracer layer, 8 nm natural Fe and 15 nm FeMn layer. Due to the almost 47 times lower density of ^{57}Fe nuclei in the natural Fe layer, the 8.5 nm (or 8 nm) of natural Fe is equivalent to about 0.18 nm (or 0.17 nm) of enriched ^{57}Fe layer, which has to be added to the artificially grown 1.5 nm (or 2 nm) ^{57}Fe tracer layer. The fcc unit cell of FeMn (with assumed lattice parameter of 0.36 nm) contains 2 Fe atoms. The same number of Fe atoms occupies the almost two times lower volume of the bcc unit cell of Fe (with assumed lattice parameter of 0.28 nm). For the same film area, the equivalent thickness of the bcc Fe structure containing the same number of Fe atoms as the FeMn fcc structure should be half of the thickness of the FeMn layer. For the analyzed FeMn films of 15 nm thickness, the equivalent thickness of the bcc structure of natural Fe will be 7.5 nm, which means about 0.15 nm of enriched ^{57}Fe layer. This equivalent thickness has to be additionally added in case of the stacks with FeMn AF films, in order to obtain an overall enriched thickness (t_e). Accordingly, the overall Mössbauer signal corresponds always to t_e. The different effective thicknesses related to the interfacial diffusion mechanisms can be evaluated by considering the relative spectral contributions of the inner sextet or of the central component in terms of relative fractions of the overall enriched ^{57}Fe thickness. Hence, $t^p_{eff} = t^*_e RA_{S2}$ and $t^d_{eff} = t^*_e RA_{CS}$, where RA_{S2} and RA_{CS} represent the relative area of the inner sextet and of the central singlet, respectively. One has to realize that this procedure involves implicitly the same escape probability (described by the weight function $T_t(z)$ [14]) for electrons leaving the stack, from the ^{57}Fe tracer layer and the other layers containing natural Fe, respectively. The maximum depth difference between the ^{57}Fe tracer layer and the most distant layer containing natural Fe is about 25 nm and correspond to the FeMn layer in sample FeMn_04. This implies a maximum variation in the weight function, $T_t(z)$, of only 15% [15], involving a similar maximum error in the estimation of the equivalent thickness for the FeMn films (an even smaller correction should be applied to the estimated equivalent thicknesses for the Fe layers). The relative area of the spectral components, the overall enriched thickness, the thickness of the ^{57}Fe tracer layer and the different effective thicknesses for each sample are presented in Table 1. The effective thicknesses are given with a precision of 0.05 nm, in order to include both the slight differences between the escape probabilities for conversion electrons starting from different depths in the stack as well as the statistical errors of the relative spectral areas. The signal coming from the natural Fe layers was assumed to contribute only to the outer sextet, whereas the signal originating from the deep FeMn layer was assumed to contribute additionally to the singlet component.

In order to compare the diffusion effects in different samples, one has to recall that the diffusion of the ^{57}Fe atoms from the tracer layer into the Cu conductive layer (or the AF layer) is connected with t^d_{eff}, and the diffusion of Cu atoms from the conductive Cu layer (or of the smaller Mn atoms from the AF layer) into the Fe tracer layer is connected with t^p_{eff}. As observed from the t^d_{eff} values of Table 1, in case of the FeMn based stacks, the diffusion of Fe atoms from the bottom F layer into the conductive Cu layer (FeMn_02) is stronger than the diffusion from the top F layer (FeMn_04). Regarding to the IrMn based multilayers, the diffusion of Fe atoms from the F layer into the Cu conductive layer is practically negligible and independent of the position of the F layer with respect to the Cu layer (samples IrMn_02 and IrMn_04).

The penetration of the Cu atoms inside the Fe layers (accounted by t^p_{eff}) is almost similar in FeMn based stacks, independent from the top or bottom position of the Fe layer (see samples FeMn_02 and FeMn_04 in Table 1). Contrary, in IrMn based multilayers, the penetration of the Cu atoms inside the top Fe layer is sensibly lower than inside the bottom Fe layer (see samples IrMn_02 and IrMn_04 in Table 1). However, the number of Fe atoms which are influenced by the penetration of Cu inside the Fe layers is larger than the number of Fe atoms diffusing inside the Cu layer (always $t^p_{eff} > t^d_{eff}$).

At this point we recall that the effective thickness of diffusing Fe atoms (t^d_{eff}) was obtained from the spectral contribution of the broad central singlet in the Mössbauer spectra, assigned to Fe atoms

Table 1
Relative area of spectral components (S1 = outer sextet; S2 = inner sextet; CS = central singlet), overall enriched thickness (t_e), thickness of the ^{57}Fe tracer layer (t_t), effective thickness of diffusing Fe atoms (t^d_{eff}), and effective thickness of perturbed Fe atoms (t^p_{eff}), as deduced from the room-temperature Mössbauer data. In case of FeMn based systems, the effective thickness, t^d_{eff}, was corrected by −0.13 nm, subtracting so the additional contribution of the deep FeMn thick layer to the Mössbauer singlet.

Sample	Spectral component	Rel. area (%)	t_e (nm)	t_t (nm)	t^d_{eff} (nm)	t^p_{eff} (nm)
FeMn_02	S1	55 (2)	1.80	1.50	0.15	0.55
	S2	29 (1)				
	CS	16 (1)				
FeMn_03	S1	40 (1)	1.80	1.50	0.35	0.55
	S2	32 (2)				
	CS	28 (2)				
FeMn_04	S1	67 (1)	2.30	2.00	0.05	0.60
	S2	27 (1)				
	CS	6 (2)				
IrMn_02	S1	69 (1)	1.70	1.50	0.05	0.50
	S2	28 (2)				
	CS	3 (2)				
IrMn_03	S1	62 (1)	1.70	1.50	0.20	0.45
	S2	26 (1)				
	CS	11 (1)				
IrMn_04	S1	83 (1)	2.20	2.00	0.05	0.30
	S2	14 (2)				
	CS	2 (2)				

penetrating the Cu layer. According to earlier Mössbauer studies on iron precipitates in CuFe alloys [16,17 and references herein] singlet like patterns could be assigned to two Fe positions: (i) either to Fe monomers in the fcc Cu lattice or (ii) to fcc γ-Fe like precipitates. The two Mossbauer patterns differ mainly by their isomer shift values which are quite close to +0.15 mm/s for case (i) and −0.1 mm/s for case (ii). Taking into account the previously mentioned isomer shifts assigned to the singlet patterns in the Mossbauer spectra of the analysed samples, it may be concluded that in FeMn based systems, Fe atoms form fcc γ-Fe like precipitates as soon as they diffuse into the Cu layer whereas in IrMn based systems, they remain as monomers. It is worth mentioning that a broad singlet with an isomer shift of −0.1 mm/s is also a characteristic of the fcc $Fe_{50}Mn_{50}$ phase [18], sustaining so the double origin of the central component in the Mössbauer spectra of the FeMn based multilayer structures.

The interfacial diffusion at the F/AF interface can be discussed with respect to the same effective thickness, but following samples FeMn_03 or IrMn_03. Firstly, one can mention that the diffusion of the Fe atoms into the AF layer is much stronger than into the Cu layer (t_{eff}^{P}, Table 1). In addition it is stronger at the Fe/FeMn interface than at the Fe/IrMn one, as observed from the t_{eff}^{d} values corresponding to samples IrMn_03 and FeMn_03. Also the penetration of the Mn atoms from the AF layer inside the F Fe layer is slightly stronger in the FeMn system as compared to the IrMn one (t_{eff}^{P}, Table 1). However, the effective thickness of perturbed Fe atoms in the F layer is comparable at both F/AF and F/Cu interfaces.

4. Conclusions

Spin-valve structures with $Fe_{50}Mn_{50}$ and $Ir_{50}Mn_{50}$ antiferromagnetic pinning layers and Cu conductive spacer layers located between the pinned and the free Fe ferromagnetic layers have been prepared by MBE. Tracer layers enriched in ^{57}Fe were placed at different interfaces. An indirect study of each interface via Mössbauer spectroscopy with conversion electrons was considered, starting from the assumption that a lower interfacial diffusion can be related to a sharper interface.

The diffusion of the Fe atoms inside of the Cu or the AF layer was estimated via the relative area of the central doublet in the Mössbauer spectrum, whereas the penetration of the Cu or Mn atoms inside the ferromagnetic layer was estimated via the relative area of the inner sextet. The Mössbauer spectra prove clearly that the ferromagnetic layers of systems prepared by MBE are definitely much better crystallized as compared to the case of systems prepared by rf. sputtering [11].

The study of the interfacial atomic diffusion by CEMS with ^{57}Fe tracer layers revealed sharper Fe/Cu interfaces in systems with IrMn films as compared to systems with FeMn films. The interfaces from the ferromagnetic side are influenced to a higher extent by the penetration of Cu or Mn atoms whereas the Cu layers are influenced to a lower extent by the diffusion of Fe atoms, especially from the top F layer. A fast Fe clustering process leading to the formation of γ-Fe fcc clusters inside the conductive Cu layer was observed for the FeMn based systems, at variance with the IrMn ones, where Fe monomers are mainly formed in the Cu layer. It seems that the interdiffusion process in the Fe/Cu/Fe structure is directly related to the type of the AF layer. Also, the interdiffusion at the F/AF interface is stronger in FeMn based systems, as compared to IrMn based ones.

It is concluded that spin-valve systems with IrMn AF layers are more convenient than similar systems based on FeMn AF layers, not only with respect to the enhanced performances related to the exchange bias effect at the F/AF interface (higher interfacial exchange energy at the F/AF interface, higher blocking temperature and lower critical thickness) but also with respect to the quality of all interfaces, including the ones of the F/Cu/F trilayer, with direct influence on the spin dependent electron transport through the conductive layer.

Acknowledgements

The work at Bucharest was supported by the National Agency for Scientific Research, Project PNII-032/2007 and at Duisburg-Essen by the Deutsche Forschungsgemeinschaft (SFB 491).

References

[1] I.R. McFadyen, E.E. Fullerton, M.J. Carey, MRS Bull. 31 (2006) 379.
[2] H.J. Richter, S.D. Harkness, MRS Bull. 31 (2006) 384.
[3] S.A. Wolf, D. Treger, A. Chtchelkanova, MRS Bull. 31 (2006) 400.
[4] B. Dieny, in: M. Johnson (Ed.), Magnetoelectronics, Elsevier, Amsterdam, 2004, p. 67.
[5] S.S.P. Parkin, MRS Bull. 31 (2006) 389.
[6] W.H. Meiklejohn, C.P. Bean, Phys. Rev. 102 (1956) 1413.
[7] Noguès, I.K. Schuller, J. Magn. Magn. Mater. 192 (1999) 203.
[8] F. Stromberg, W. Keune, V. Kuncser, K. Westerholt, Phys. Rev. B 72 (2005) 064440.
[9] F. Radu, H. Zabel, in: H. Zabel, S.D. Bader (Eds.), Magnetic Heterostructures, Advances and Perspectives in Spinstructures and Spintransport, Springer Tracts in Modern Physics, 227, Springer, Berlin Heidelberg, 2008, p. 97.
[10] V. Kuncser, M. Valeanu, G. Schinteie, I. Mustata, C.P. Lungu, A. Anghel, H. Chiriac, R. Vladoiu, J. Bartolome, J. Magn. Magn. Mater. 320 (2008) e226.
[11] V. Kuncser, G. Schinteie, P. Palade, I. Mustata, C.P. Lungu, N. Stefan, H. Chiriac, R. Vladoiu, G. Filoti, Hyperfine Interact. 191 (2009) 135.
[12] R.A. Brand, Nucl. Instrum. Methods Phys. Res., Sect. B 28 (1987) 398.
[13] K. Sumiyama, Y. Nakamura, K. Tanaka, Hyperfine Interact. 53 (1990) 143.
[14] D. Liljequist, T. Ekdahl, U. Baverstam, Nucl. Instrum. Methods 155 (1978) 529.
[15] V.E. Kuncser, M. Doi, W. Keune, M. Askin, H. Spies, J.S. Jiang, A. Inomata, S.D. Bader, Phys. Rev B 68 (2003) 064416.
[16] S.J. Campbell, P.E. Clark, J. Phys. F.:Metal Phys. 4 (1974) 1073.
[17] V. Kuncser, M. Rosenberg, A.R. Yavari, G. Filoti, J. Alloys Compd. 289 (1999) 270.
[18] T.A. Anhoj, C.S. Jacobsen, S. Morup, J. Appl. Phys. 957 (2004) 3649.